Available online at www.sciencedirect.com
SCIENCE DIRECT®
Aerosol Science 36 (2005) 1108–1124
Journal of Aerosol Science
www.elsevier.com/locate/jaerosci

Comparing aerosol surface-area measurements of monodisperse ultrafine silver agglomerates by mobility analysis, transmission electron microscopy and diffusion charging

Bon Ki Ku, Andrew D. Maynard*

Centers for Disease Control and Prevention, National Institute for Occupational Safety and Health (NIOSH), 4676 Columbia Parkway, MS-R3, Cincinnati, Ohio 45226, USA

Received 14 June 2004; accepted 3 December 2004

Abstract

Three methods—scanning mobility particle sizer (SMPS), transmission electron microscopy (TEM), and diffusion charging (DC)—for estimating aerosol surface area were evaluated and compared. The aerosol used was monodisperse silver particles, having morphologies that range from spherical to agglomerated particles, with corresponding fractal dimensions from 1.58 to 1.94. For monodisperse silver particle agglomerates smaller than 100 nm, the DC response was proportional to the mobility diameter squared, regardless of morphology. For particle sizes from 80 to 200 nm, the DC response varied as the mobility diameter to the power 1.5. The projected surface area of agglomerates analyzed by TEM agreed well with that estimated from particle mobility diameters for particles smaller than 100 nm. The surface area of monodisperse particles, measured by DC and SMPS, was comparable to the geometric surface area below 100 nm, but in the size range of 100–200 nm, the methods used underestimated the geometric surface area. SMPS, TEM, and DC-based measurements of surface area were in good agreement with one another for monodisperse aerosol particles smaller than 100 nm.
Published by Elsevier Ltd.

Keywords: Aerosol surface area; Diffusion charging; Silver agglomerates

* Corresponding author. Tel.: +1 513 841 4319; fax: +1 513 841 4545.
E-mail address: amaynard@cdc.gov (A.D. Maynard).

0021-8502/$ - see front matter Published by Elsevier Ltd.
doi:10.1016/j.jaerosci.2004.12.003

1. Introduction

The toxicity of most inhaled aerosol particles is generally accepted to be associated with particulate mass. However, several studies in recent years have indicated that the toxicity of low-solubility inhaled particles may be more appropriately associated with particulate surface area (Oberdörster, Gelein, Ferin, & Weiss, 1995; Oberdörster, 2000; Brown, Wilson, MacNee, Stone, & Donaldson, 2001). Ultrafine particles (particles below 100 nm) have a higher specific surface area (area unit per mass) than coarser particles, and it is plausible that evaluating exposures to such particles by their mass concentration may lead to the underestimation of health risks. While this hypothesis probably will not gain wide approval until extensive data relate occupational health effects to aerosol surface area, intuitively, an association between the surface area of insoluble lung deposits and health effects is anticipated.

Although workplace exposures to ultrafine particles are widespread and predicted to increase due to the advent of mainstream nanotechnology, the means of measuring aerosol exposures in terms of surface area are not readily available. The standard method for measuring surface area (the Brunauer–Emmett–Teller (BET) method (Brunauer, Emmett, & Teller, 1938)) is appropriate for relatively large quantities of powder only, but not suited to a rapid evaluation of aerosol surface area, particularly at low concentrations.

Research to find alternative methods for analyzing nanotechnology exposures from ultrafine particles in the workplace is ongoing. Woo, Chen, Pui, and Wilson (2001) and Maynard (2003) have estimated surface area from measurements of number and mass concentration and, in the case of Woo et al. (2001) charge measurement. However, while these two methods may be suitable for rough estimates of surface area concentration, they are not designed for accurate exposure measurements in this emerging technology.

Other possible methods and instruments for measuring aerosol surface area include the diffusion charging (DC), transmission electron microscopy (TEM), and scanning mobility particle sizer (SMPS). Recently, Bukowiecki et al. (2002) used real-time instruments, including DC and particle counter, for characterizing combustion aerosols in the air. These experiments showed the possibilities offered by DC for the real-time monitoring of ambient aerosols.

In the present paper, three techniques—DC, TEM, and SMPS—for estimating aerosol surface area are evaluated and compared. Monodisperse silver particle agglomerates were used as the test aerosol. In addition, the responses from two DC models were investigated systematically for various particle morphologies. Unlike BET, these techniques are only sensitive to the outer surface of particles being assessed.

2. Theory

Active (Fuchs, 1963) surface area is defined as the surface of a particle that is involved in interactions with the surrounding gas. In the free molecular regime, active surface area is equivalent to geometric surface area for spherical particles. Because particle mobility and molecule attachment rate are governed by particle–molecule collisions, it is theoretically possible to use either quantity to measure the active surface area. Rogak, Flagan, and Nguyen (1993) demonstrated that for mobility diameters smaller than 400 nm (extending well into the transition regime), the equivalent sphere projected area diameter (the diameter of a sphere having the same projected area) of particles scaled with the particle mobility diameter for fractal-like particles. Similarly, Keller, Fierz, Siegmann, Siegmann, and Filippov (2001) showed that

the product of ion attachment coefficient K and mobility Z was nearly constant in the size range from 20 to 180 nm.

Singly charged aerosol particle electrical mobility Z may be expressed as

$$Z = \frac{eC(Kn)}{3\pi\eta d}, \tag{1}$$

where $C(Kn) = 1 + Kn[1.257 + 0.4\exp(-1.1/Kn)]$ (Friedlander, 1977) where η is the viscosity of the gas, $C(Kn)$ the slip correction factor at Knudsen number Kn (defined as $2\lambda/d$), d the particle's mobility diameter, and e the elementary charge. λ is the mean free path of the carrier gas. The electrical mobility of a singly charged particle selected by a concentric geometry Differential Mobility Analyzer (DMA), such as the model 3081 (TSI, Inc., St. Paul, MN) is given by

$$Z = \frac{q_c \ln(r_2/r_1)}{2\pi V L}, \tag{2}$$

where r_1 and r_2 are the radii of the inner electrode and outer electrode, respectively, L is the length of electrodes, V the voltage difference between the two electrodes, and q_c the clean sheath gas flow rate in the DMA. In the free molecular regime ($Kn \gg 1$), Eq. (1) becomes

$$Z = \frac{1.105e\lambda}{\eta\pi d^2}. \tag{3}$$

Thus, combining Eqs. (2) and (3), it can be seen that in the free molecular regime, the projected surface area $A(\pi d^2/4)$ is directly related to DMA voltage

$$A = \frac{0.5525\pi e\lambda L}{\eta q_c \ln(r_2/r_1)}\, V. \tag{4}$$

For diffusion charging of particles of a given size in a unipolar ion cloud, the ion attachment rate onto neutral particles may be expressed as

$$\frac{dn}{dt} = -KNn, \tag{5}$$

(Baron & Willeke, 2001) where n is the ion concentration, N the concentration of monodisperse particles of diameter d, and K the mass transfer coefficient (or ion attachment coefficient).

In the free molecular regime, K is given by

$$K = \overline{v}\,\frac{\pi}{4}\,d^2, \tag{6}$$

(Siegmann & Siegmann, 2000) where $\overline{v}$ is the average velocity of the ions, $(3kT/m)^{1/2}$, m the ion mass, k the Boltzmann's constant, and T the absolute temperature.

Replacing $\pi d^2/4$ by projected surface area A and combining Eqs. (5) and (6) yield

$$A = \frac{1}{\sqrt{(3kT/m)Nn}}\,\frac{dn}{dt}. \tag{7}$$

Keller et al. (2001) showed that the product of ion attachment coefficient K and mobility is nearly constant in the size range from 20 to 180 nm, indicating that K scales with $1/Z$ in this size range and

in turn with d^2 in the free molecular regime (Eq. (6)). Aerosol charging rate in a unipolar ion cloud due to ion diffusion can be assumed to be governed by K as long as the charge per particle remains low (i.e., multiple charging is negligible). Thus, diffusion charging can be used as a basis for measuring particle surface area in the free molecular regime. For $Kn < 1$, diffusion charging is associated with Fuchs surface (Keller et al., 2001) and is expected to vary as d^1 for $Kn \ll 1$. From the relationship between Z and K, measurements of aerosol surface area for particles smaller than 180 nm in diameter should be comparable when diffusion charging and mobility analysis are used with Eqs. (4) and (7). In addition, Eq. (4) indicates that DMA voltage can be used to determine the projected surface area of selected particles, allowing a simple determination of aerosol surface area in the free molecular regime. Because mobility diameter is governed by particle–molecule collisions, it is to be expected that DMA voltage-determined aerosol surface area provides an indication of Fuchs surface area for $Kn < 1$.

3. Experimental details

3.1. Aerosol generation

To investigate the response from a range of surface area measurement instruments and methods for monodisperse particles covering a range of sizes and morphologies, a test facility was constructed (Fig. 1) (Ku & Maynard, 2004). Silver (Ag) particles covering a range of diameters and morphologies were generated by two horizontal tube furnaces in series. Silver wire (purity level 99.9%) was placed in a ceramic boat in the first furnace and heated at 1200 °C in a pure nitrogen atmosphere (purity level 99.999%).

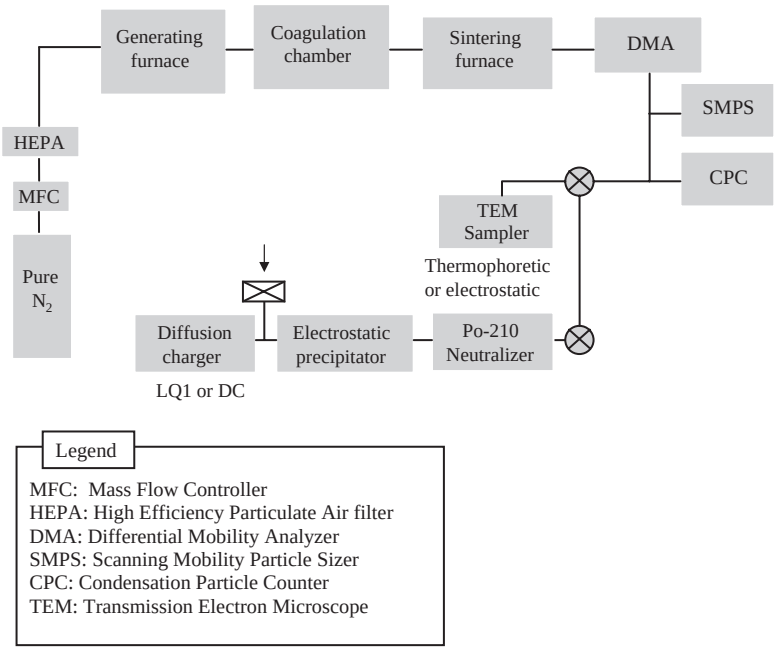

Fig. 1. Experimental setup to generate monodisperse silver particles, and evaluate instrument response.

The nitrogen was passed through the furnace at a flow rate of 1.0 lpm, controlled by a digital mass flow controller (Brooks Instrument, USA.: Model 0154). Particle formation within the first furnace was primarily by homogeneous nucleation. The aerosol leaving this furnace was allowed to age in a coagulation chamber (residence time about 40 s), leading to the formation of agglomerates with low fractal dimensions. The second tube furnace was operated at different temperatures to provide either partial or complete sintering of agglomerates or coalescence, thus, allowing some degree of control over particle morphology. Particles of specific mobility diameters were subsequently selected with a Differential Mobility Analyzer (DMA-Model 3081, TSI, Inc.) before they were characterized by an array of techniques. For all the experiments, the aerosol flow rate was fixed at 1.0 lpm and the sintering temperature varied from room temperature (no sintering, 20 °C) to 700 °C. The DMA was calibrated with standard PSL (Polystyrene Latex) particles of 20 and 100 nm (Duke Scientific Co.). The equivalent sphere projected area, calculated from the selected particle mobility diameter ($\pi d_m^2/4$), was chosen as the reference particle surface area, allowing direct comparison with TEM results.

3.2. Surface area measurement instruments

3.2.1. Mobility analysis

An SMPS (TSI, St Paul, MN) was used to estimate aerosol surface area from the measured size distribution. Under the assumption that spherical particles had a physical diameter equivalent to their mobility diameter, the aerosol surface area was determined by the size distributions. Eq. (4) was also used to calculate aerosol surface area directly from DMA voltage and, thus, give an estimated surface area by integrating the resultant surface-area weighted distribution. Results were reported as a mean projected surface area per particle, which allowed direct comparison with TEM data.

3.2.2. Collection and analysis in the TEM

Although TEM analysis is limited due to a two-dimensional projection of particles, it was anticipated that for the particle morphologies under consideration, image analysis would allow for derivation of a reasonable estimate of physical surface area. Aerosol samples were collected either electrostatically or thermophoretically for at least 1 h. The thermophoretic precipitator used is described by Maynard (1995) and was designed to provide an even distribution of particles on a TEM support grid. Sampling was carried out at a flow rate of 0.7 l/min and a temperature gradient of 6×10^5 °C/m for typically 60 min. Electrostatic sampling was carried out using an electrostatically enhanced impactor. A TSI SMPS inlet impactor (Part No. 1502296) with a 0.508 mm orifice (50% cut size: 1.006 μm at 0.2 lpm) was modified to allow for placement of a 3 mm TEM grid below the orifice, and for establishment of an electrostatic field between the orifice and the grid (Fig. 2). The sampler was operated at 0.1 l/min, under an applied voltage of 2.2 kV.

The TEM sampler was placed after the DMA, in parallel with a Condensation Particle Counter (CPC). Aerosol flow rate leaving the DMA was 1.0 lpm and split into the CPC (0.3 lpm) and TEM sampling units (0.7 lpm). For electrostatic sampling, the flow rate was reduced to about 0.1 lpm to improve the collection efficiency of larger particles.

Particle imaging was carried out using a Philips EM420 Transmission Electron Microscope. The TEM magnification was calibrated by a grating replica (TED Pella Inc.). During the TEM analysis, agglomerates were selected and imaged randomly to minimize bias. Magnifications between $79,000X$ and $96,000X$ were typically used, giving three to five particles per image. For each sample, six to ten

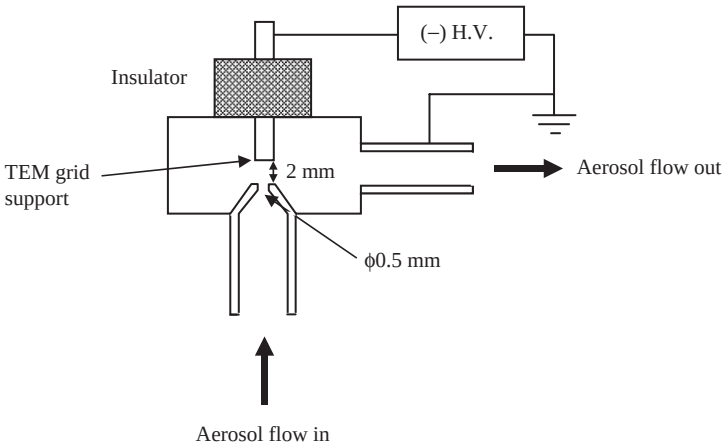

Fig. 2. Schematic of the electrostatic TEM sampler constructed.

fields of view were used to estimate aerosol surface area. Micrographs were taken with a CCD (Charge Coupled Device) camera (Multiscan Camera Model 791, Gatan), giving 1024 by 1024 pixel, 14 bit images. TEM projected surface area distribution was obtained, first, by thresholding the original TEM image and, next, by calculating the projected surface area of each particle. Image processing was carried out using ImageJ, a public domain image analysis program, which was developed at the National Institutes of Health. Good image processing of the gray-level image depends on background shading and extraneous structures in the image. For this reason, the boundary of each particle was located manually before it was thresholded. The projected surface area measured from the resulting binary image varied by ±4% due to ambiguity in the agglomerate boundary. Measured agglomerate surface area was normalized by the number of particles analyzed, for each particle mobility diameter, to give a mean projected surface area per particle.

3.2.3. Diffusion charging

Two DC models were used to measure particle surface area. The LQ1-DC (Matter Engineering, Wohlen, Switzerland) is a bench-top unit, while the DC2000CE (EcoChem, USA) is a smaller portable unit. Both instruments tested had a quoted range of 0–2000 $\mu m^2/cm^3$, and a sensitivity of 1 $\mu m^2/cm^3$. Each exposed the sampled aerosol to a positive ion cloud before collecting the particles on a filter and measuring the charge. The instruments were placed in parallel with a CPC and challenged with mobility-selected particles. To avoid artifacts associated with sampling charged particles in the DCs, a neutralizer ($2 \times$ 500 μCi Po-210) was connected to their inlets. A charged particle trap consisting of two parallel electrodes sustaining an electric field was also placed in-line with DCs, with the thought of ensuring measured response to charge-neutral particles. However, the trap was found to be relatively ineffective, with only 5–10% particle losses occurring within the neutralizer and trap at 200 nm.

In this study, the response from each DC was averaged over five samples obtained under the same experimental conditions. Measured aerosol surface area was normalized by particle number concentration and divided by a factor of 4 to give the equivalent sphere projected surface area. The aerosol surface area was reported as the mean projected surface area per particle for direct comparison with TEM data.

4. Results and discussion

4.1. Comparison of projected surface area of monodisperse particles measured by diffusion chargers, SMPS, and TEM

Projected area data measured by two DCs, SMPS (assuming spherical particles), and TEM are compared in Fig. 3. The data represent particles having mobility diameters between 20 and 100 nm. Particles having the highest surface area—100 nm—were sintered at 300 °C. For all other measurements, the particles were not sintered. The equivalent projected surface area in Fig. 3 was calculated from the mobility diameter. Estimations of surface area from different instrument measurements agreed with one another. This fact indicated that in the ultrafine particle size range (typically below 100 nm), projected surface can be estimated quite well, based on diffusion charging, mobility analysis, and electron microscopy. It also confirmed the theoretical idea that in the free molecular regime, surface area of particles determines the interactions between particles and molecules or ions, and, thus, either technique—mobility analysis or diffusion charging—is applicable to measuring aerosol surface area. In addition, this result was quite promising in that the DC and SMPS data can be used to measure surface area of ultrafine aerosols generated in the workplace in situ, while TEM data can be supplied to confirm the surface area measurements of the two instruments.

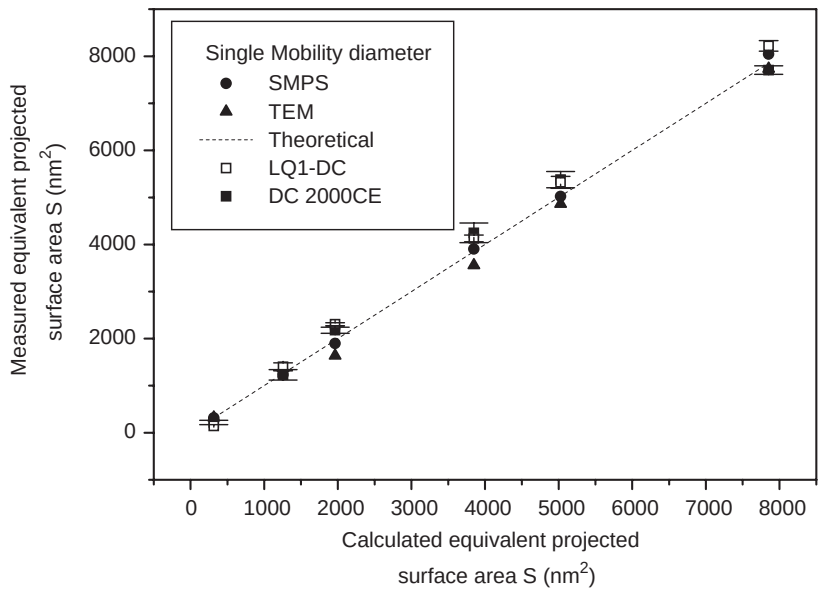

Fig. 3. Comparison of surface-area measurements of monodisperse agglomerates. Plotted data represent particles with mobility diameters between 20 and 100 nm. One hundred nanometer particles (highest surface area) were sintered at 300 °C: for all other measurements the aerosol was not sintered. Measured projected surface area was normalized by the number of particles analyzed for each particle mobility diameter, to give a mean projected surface area per particle. Equivalent projected surface area is calculated from particle mobility diameter.

4.2. Comparison of projected surface area of monodisperse particles measured by SMPS and TEM

Fig. 4 shows normalized number concentration versus projected surface area, as measured by SMPS (assuming spheres) and TEM for six monodisperse aerosols. Twenty nanometer particles from the generation system were spherical without sintering. At larger mobility diameters, measured fractal dimension decreased with increasing diameter, as shown in Fig. 5. Corresponding fractal dimensions for particles in Fig. 5 are 1.94 ± 0.02 for 20 nm and 1.58 ± 0.02 for 80 nm, based on calculations by ImageJ program. In Fig. 4, normalized distributions for all the particle sizes are in good agreement with each other. The projected surface area measured by TEM was almost equivalent to the projected surface area calculated from SMPS size distribution assuming a spherical particle of the same mobility diameter as the agglomerate, regardless of particle morphology. These results, confirming the findings of Rogak et al. (1993), indicated that the mobility diameter of agglomerated particle can be regarded as the diameter of a sphere having the same projected area.

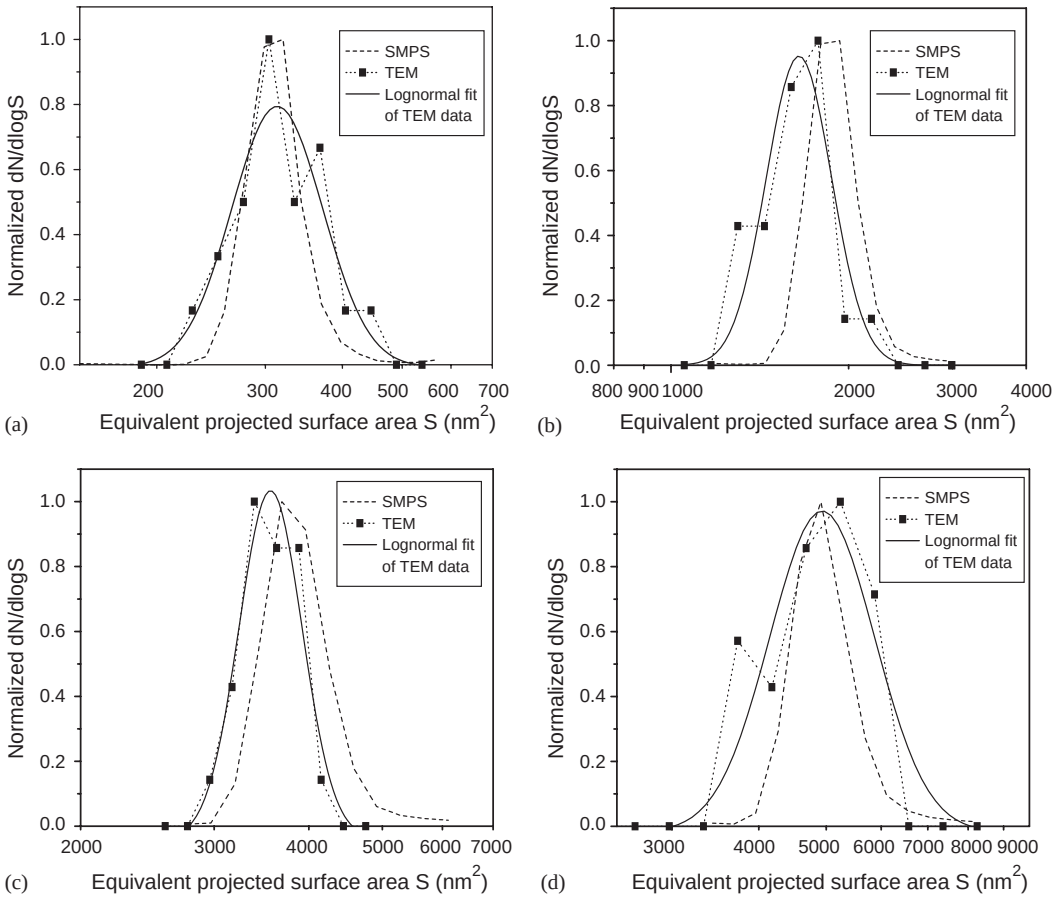

Fig. 4. Comparison of projected surface area of un-sintered monodisperse particles measured by TEM with that measured using the SMPS assuming spherical particles: (a) 20 nm mobility diameter particles, (b) 50 nm mobility diameter particles, (c) 70 nm mobility diameter particles, (d) 80 nm mobility diameter particles.

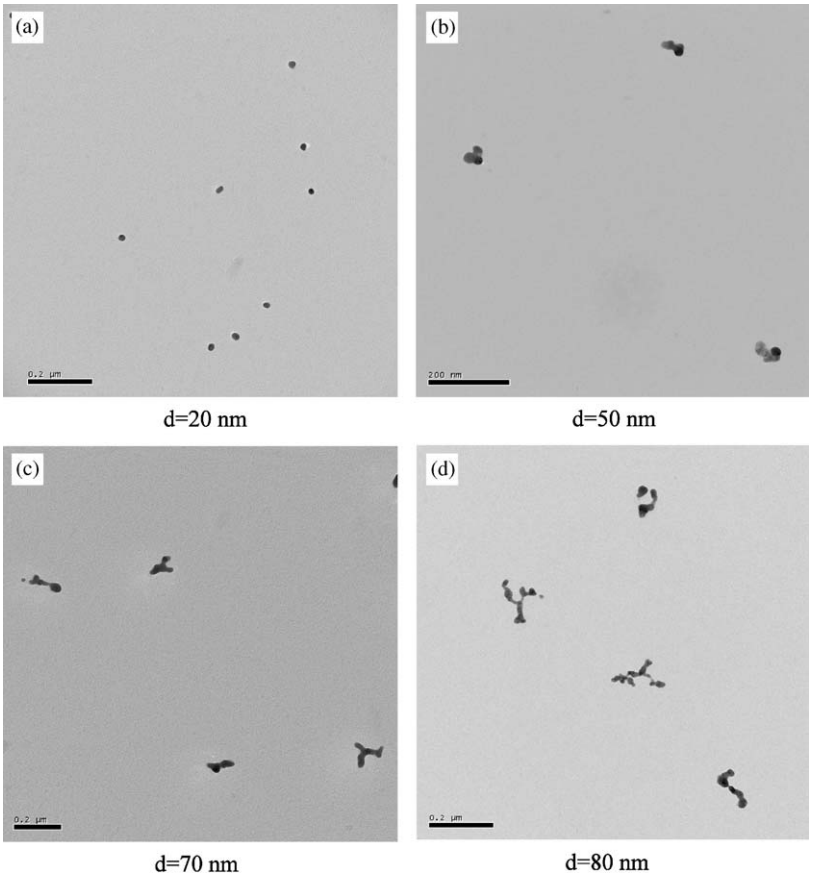

Fig. 5. Particle morphologies of agglomerates with single mobility diameters. Projected area fractal dimensions for these agglomerates are: (a) 1.94 ± 0.02, (b) 1.75 ± 0.01, (c) 1.67 ± 0.04, (d) 1.58 ± 0.02.

4.3. Diffusion charger response to particle size and morphology

Fig. 6 shows the DC responses to particles with mobility diameters of 100 nm and smaller, without sintering. The two instrument responses were approximately proportional to mobility diameter squared. A *T*-test on the fit parameter *b* (Fig. 6) gave a *P*-value of 0.061, indicating that at a significance level of 5%, the two instrument responses were identical (Table 1). Analysis of variance, accounting for instrument response as a function of particle diameter, confirmed no statistical difference between the two instruments tested (Table 1).

Fig. 7a compares aerosol surface area measurements using the DC and SMPS for particle mobility diameters up to 200 nm, sintered at 200 °C. Nominal surface area (horizontal axis) was calculated from the DMA-selected mobility diameter, assuming spherical particles. SMPS data were evaluated by integrating the calculated aerosol surface area-weighted distribution in two ways: (1) by assuming spherical particles and (2) by using the relationship between DMA voltage and surface area (Eq. (4)) in the SMPS. Below 100 nm, all three methods for estimating surface area were comparable although when DMA voltage was

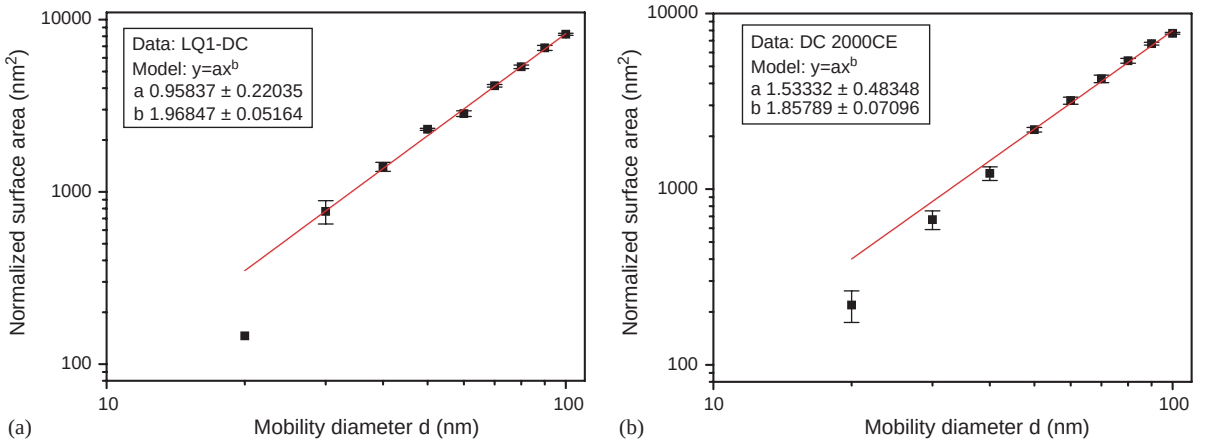

Fig. 6. Response of diffusion chargers to monodisperse agglomerates without sintering: (a) LQ1-DC, (b) DC 2000CE. Plotted data represent spherical and agglomerated particles with mobility diameters between 20 and 100 nm. Normalized surface area is obtained by dividing surface area measured from each diffusion charger by number concentration and a factor of 4 (to give projected surface area).

Table 1
Summary statistics of *T*-test and *F*-test comparing the response of two different diffusion chargers

T-test[a]

Hypothesis	Degree of freedom	*t* value	$P(T > \|t\|)$
Both instruments are equivalent	41	1.93	0.061

F-test (analysis of variance)[b]

Source	Degree of freedom (DF)	Sum of squares (SS)	Mean squares (MS = SS/DF)	*F* value	$P > F$
Instrument type (I)	1	1.57E4	1.57E4	0.11	0.7391
Diameter*I	1	9.97E4	9.97E4	0.71	0.4015

[a](Hogg & Tanis, 1993; Searle, 1971).
[b](Hogg & Tanis, 1993).

used, it appeared to underestimate the surface area slightly. Above 100 nm, each method increasingly underestimated the aerosol surface area. The anticipated deviation from a diameter squared relationship predicted from the slip correction factor (Eq. (1)) is 24% at 100 nm, 34% at 150 nm and 42% at 200 nm. Estimates of surface area using the SMPS (assuming spherical particles) and the diffusion charger show smaller deviations than anticipated.

The SMPS-derived surface area, assuming spherical particles, was expected to closely match the nominal surface area for the monodisperse aerosols. However, significant deviation was observed between expected and measured values above 100 nm. Closer examination of the measured aerosol size distributions showed significant multiple charging in the SMPS-measured aerosol, which would have led to an underestimation of the aerosol surface area. Multiple charging was significant above mobility diameters of 100 nm. Fig. 7b shows a typical size distribution for 200 nm diameter monodisperse particles. Doubly and triply charged particles appear to the left of singly charged particles, peaking at 200 nm. The absence

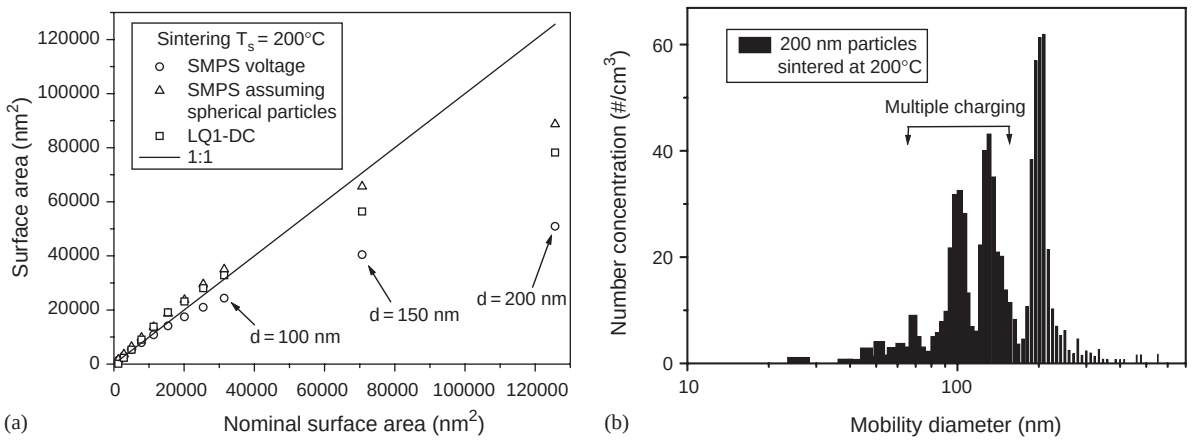

Fig. 7. (a) Comparison of nominal surface area of monodisperse agglomerates with measured surface area. Plotted data represent particles with mobility diameters between 20 and 200 nm. Nominal surface area is calculated assuming spherical particles. (b) SMPS-measured size distribution of monodisperse agglomerates of mobility diameter 200 nm sintered at 200 °C, showing the presence of significant numbers of multiply charged particles.

of peaks above 200 nm indicates that multiple charging was primarily occurring in the SMPS, and not the DMA that was used to select the monodisperse particles.

The percentage of multiply charged particles observed was higher than theoretically expected from 200 nm particles by approximately a factor of 5. The increased probability of multiple charging might be slightly associated with the lower charge-to-surface ratio in the agglomerates of 200 nm with lower fractal dimension, compared to comparable spheres. For instance, Rogak and Flagan (1992) reported that agglomerates in a bipolar DC had a 5% higher charged fraction than spherical particles in sizes ranging from 100 to 800 nm. However, this is insufficient to explain the magnitude of the phenomenon observed here. While it is clear that multiple charging influenced the derivation of aerosol surface area from SMPS data in this instance, it is unclear whether this will be repeatable within other experimental setups.

Using SMPS voltage to estimate aerosol surface area led to marked underestimates of surface area above 100 nm. The relationship between DMA voltage and aerosol particle surface area in Eq. (4) assumed $Kn \gg 1$. Thus, significant deviation between actual and DMA voltage-derived surface area was expected for $Kn < 1$. DMA voltage-derived surface area would be expected to closely match the active surface area as measured by the DC. The significant deviation between estimates by this method and the DC were possibly associated with multiple charging, as discussed above. While DMA voltage should be useable in principle for estimating active surface area, our results indicated that multiple charging in some aerosols might lead to substantial underestimations.

The effect of particle morphology on DC response was comprehensively investigated by using the LQ1-DC. Particles sintered at various temperatures, ranging from 20 °C (no sintering) to 700 °C, providing different particle shapes. Typical particle shapes for different sintering temperatures are shown in Fig. 8. Most of the agglomerates sintered at 100 °C remained agglomerated, with a gradual shift to spherical particles as the temperature approached 700 °C (Fig. 8b). One hundred nanometer agglomerates retained non-spherical shapes at 300 °C (Fig. 8c) and collapsed into spheres at 600 °C (Fig. 8d). Fig. 9 shows that there is little difference in DC responses for different particle shapes. All of the data, except those at

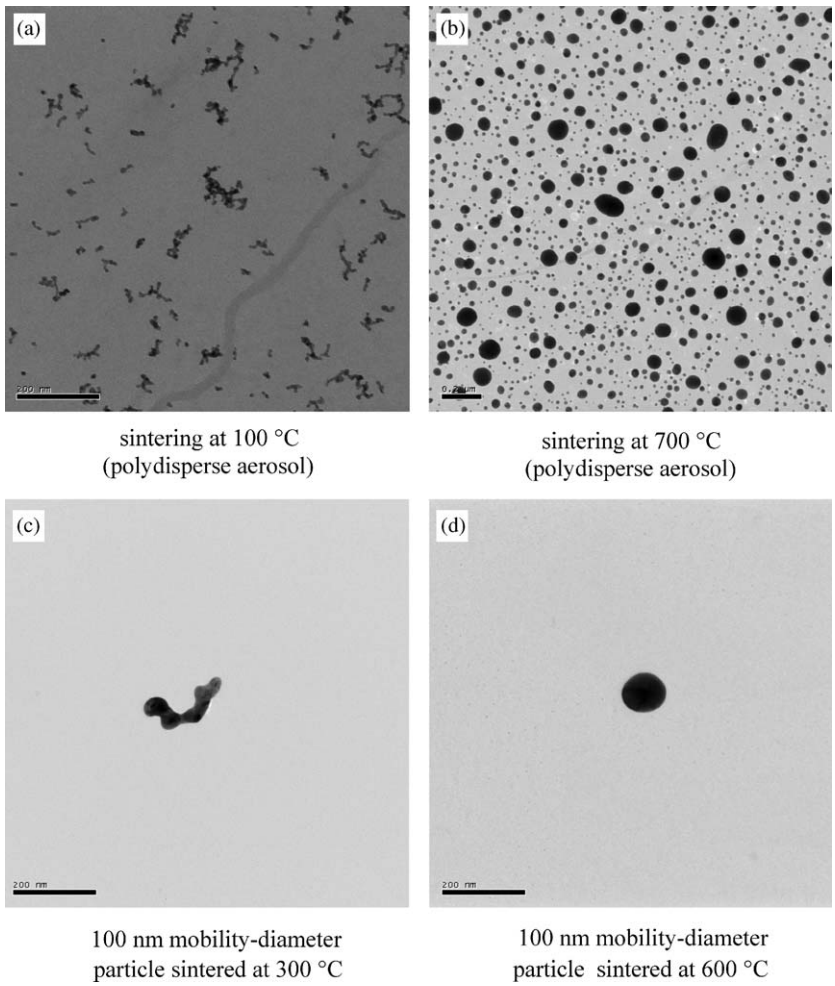

Fig. 8. Examples of particle morphologies of agglomerates for various sintering temperatures.

20 nm from the DC, are fitted well with a power model of the form $y = ax^b$ (where x is mobility diameter, y is normalized surface area, and x is in the range from 20 to 100 nm), giving power b equal to almost 2. For the 20 nm data, deviation from the fitted curve was analyzed to see if it was caused by particle loss during neutralization, before the DC. Based on our comparisons of number concentration measurements between neutralized (20–25% particle losses for 20 nm particles) and not neutralized, we concluded that the loss was not large enough to account for the smaller normalized surface area, as shown in Fig. 9. The deviation at 20 nm may have been partly due to the DC detection limit. The total surface area of 20 nm particles corresponded to $\sim$ 1–2 $\mu m^2/cm^3$. As Fig. 9 plots data on a log-to-log scale, small deviations from the expected relationship at small particle diameters are heavily emphasized.

Fig. 10 shows the DC response versus particle size extended to 200 nm. The power b decreases to 1.62 when the instrument response to particles between 20 and 200 nm is included. The change in response appears to start at a mobility diameter of 80–90 nm, corresponding to the regime where the interaction

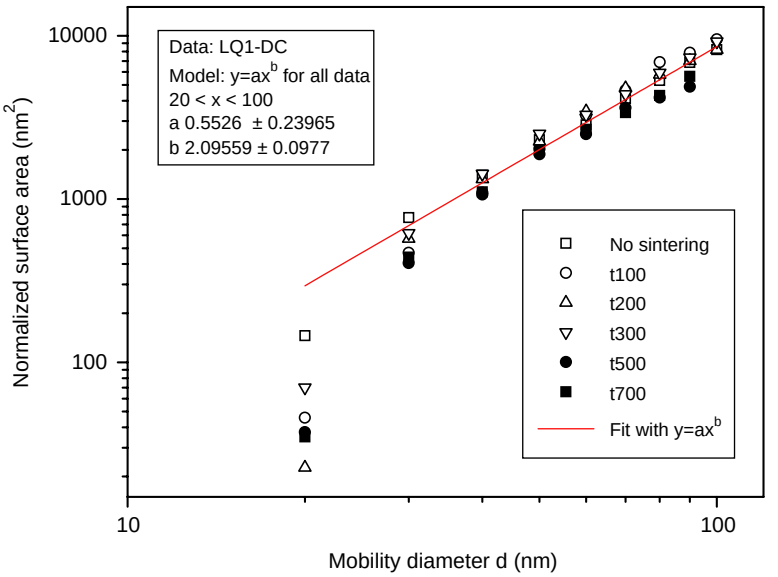

Fig. 9. Diffusion charger response to different particle shapes in the size range from 20 to 100 nm. Data are presented for sintering temperatures between 100 and 700 °C. Diffusion charger response has been normalized by particle number concentration and a factor of 4, to give projected surface area.

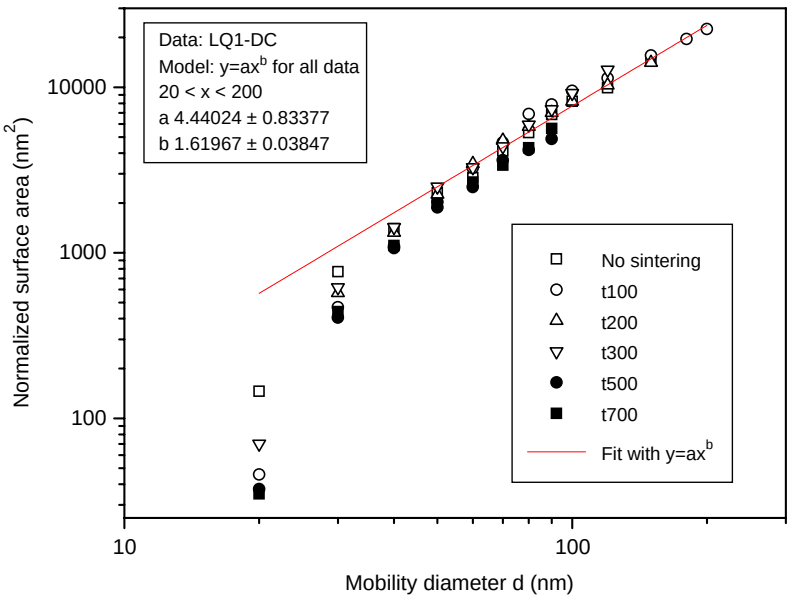

Fig. 10. Diffusion charger response to different particle shapes in the size range from 20 to 200 nm at various sintering temperatures. Surface area is normalized by particle number concentration and a factor of 4, to give projected surface area.

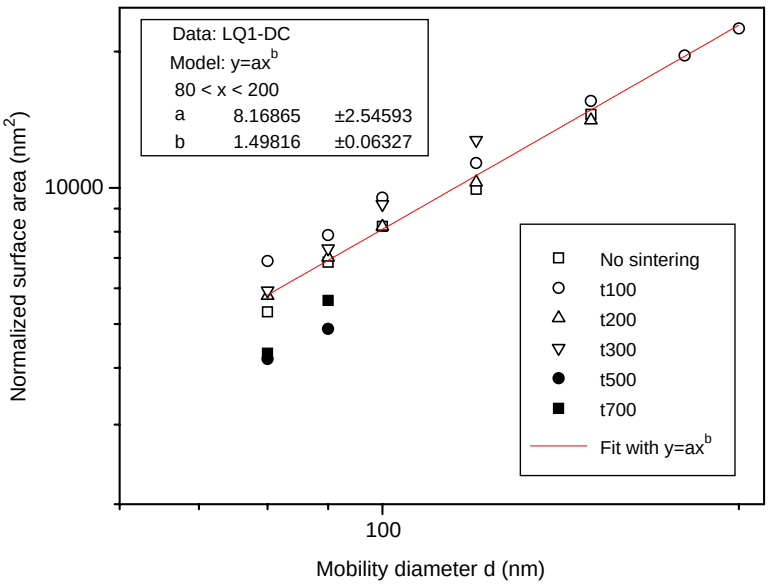

Fig. 11. Diffusion charger response to different particle shapes in the size range from 80 to 200 nm at various sintering temperatures. DC response is normalized by particle number concentration and a factor of 4, to give projected surface area.

between particles and charged ions starts to transit from molecular dynamics to diffusion dynamics. Fitting data above and below 80 nm indicates two distinct response regions, such that data above 80 nm are described by a power law, having an exponent of 1.5 (Fig. 11). Although data points above 80 nm are described well with an exponential function, the exponent value of 1.5 is most likely a function of the particle size range over which the relationship is evaluated. As particles move from the free molecular regime, through the transition regime to the continuum regime, theory dictates a continuous decrease in the exponent from 2 to 1.

Pui, Fruin, and McMurry (1988) reported that the combination coefficient between neutral particles and positive ions is related to the 1.64–1.71 power of the mobility diameter in the sizes ranging from 7 to 50 nm. Weber, Baltensperger, Gäggeler, and Schmidt-Ott (1996) identified that the attachment rate of radioactive lead clusters to silver agglomerates in the size ranging from 70–200 nm was proportional to the 1.47 power of mobility diameter with which our experimental data agreed well. Good agreement between our data and Weber et al. (1996) indicates that the relation of the attachment rate to agglomerates that have a mobility diameter in the size range of both studies is conserved independently of whether attaching species are ions or neutral clusters. Recently, Wilson, Han, Stanek, Turner, and Pui (2003) showed that the response of an electrical aerosol detector based on turbulent diffusion charging (3070A EAD, TSI) is related to the 1.16 power of the mobility diameter, by comparing charge acceptance measurements with mobility sizes and theoretical calculations. In addition, Jung and Kittelson (2004) have shown that the responses of an LQ1-DC and an EAD to NaCl particles are proportional to $d^{1.36}$ and $d^{1.13}$ of the mobility diameter d in the size range of 30–150 nm, respectively. Our data suggest a transition from a d^2 relationship below 80 nm to a $d^{1.5}$ relationship between 80 and 200 nm, thus, tentatively supporting the results of Pui et al. (1988) and Weber et al. (1996). Measurements made by Jung and Kittelson (2004)

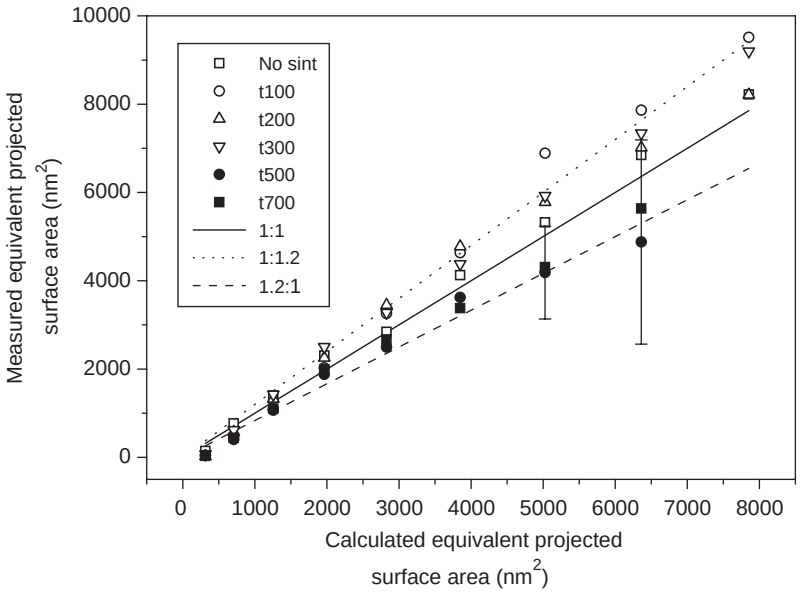

Fig. 12. Comparison of surface-area measurements of monodisperse agglomerates by diffusion charger for different sintering temperatures. Plotted data represent particles with mobility diameters between 20 and 100 nm. Measured projected surface area was normalized by the number of particles analyzed for each particle mobility diameter, to give a mean projected surface area per particle. Equivalent projected surface area is calculated from the known mobility diameter.

indicated a lower exponent and raised questions about the chemical nature of the aerosol used. All reported data on the TSI EAD indicates it had a markedly different response from the Matter Engineering DC. This response might possibly be associated with the charging arrangement in the EAD that may lead to a higher incidence of multiple charging.

Fig. 12 provides a detailed representation of DC responses for particles smaller than 100 nm, as a function of sintering temperature. Most of the surface area measurements agree with the surface area calculated by known mobility diameter regardless of particle morphologies, and the effect of particle morphology on the DC response appears to be small. Qualitatively, below 300 °C, measured projected surface area is slightly overestimated, but above 500 °C, DC and DMA-derived surface area agree within experimental errors. These results may be related to particle shapes and active surface area. Particles still have fractal-like structures below 300 °C, which may have a higher active surface area than spherical particles of the same mobility diameter. Above 500 °C, aerosol particles are almost spherical in the size range up to 100 nm; therefore, the active surface area is comparable to that of a spherical particle. In previous studies the response of the epiphaniometer showed little difference between particle morphologies, based on the attachment rate of neutral atoms to spherical particles (singlet NaCl, PSL, $(NH_4)_2SO_2$) and agglomerated particles (carbon agglomerates, TiO_2) for a given mobility diameter (Rogak, Baltensperger, & Flagan, 1991; Shi, Harrison, & Evans, 2001). However, in our study of spherical and agglomerated particles (silver particles), the attachment rate of charged ions to particles in the DC appeared to depend slightly on particle morphologies for a given mobility diameter (Fig. 12). Higher ion attachment rates were obtained from non-sintered agglomerates and partly sintered agglomerates (300 °C) than for spherical particles (500 °C and 700 °C). Rogak and Flagan (1992) reported that agglomerates in a bipolar

DC have a 5% higher charged fraction than spherical particles in the sizes ranging from 100 to 800 nm for PSL and $(NH_4)_2SO_2$ spheres and for TiO_2 agglomerates, while their charged fraction was equal to smaller-sized (40–45 nm) spherical particles. It can be hypothesized that lower fractal-dimension agglomerates entering the DC will have a lower charge-to-surface ratio than equivalent spherical particles, and thus, lead to a greater probability of multiple charging. Our observations support this hypothesis, although deviations from a d^2 response with particle morphology below a mobility diameter of 100 nm are small.

5. Conclusions

The scanning mobility particle sizer (SMPS), transmission electron microscope (TEM), and diffusion charger (DC) responses were compared to estimate the surface area of monodisperse aerosol. To evaluate the capability of the DC to represent aerosol surface area, its response to monodisperse particles with different particle morphologies was investigated. Based on the findings of our study, the following conclusions can be made:

(1) For monodisperse aerosols below 100 nm having spherical and fractal-like geometries, the DC response is proportional to the mobility diameter squared, while for particle sizes from 80 to 200 nm, the DC response deviates from the mobility diameter squared to the mobility diameter (as theoretically expected), to a power of 1.5.
(2) For monodisperse aerosol, the projected surface area, measured by TEM at a given mobility diameter, tends to be independent of whether the particles are spherical or agglomerates of smaller particles.
(3) The projected surface area of particles in the size range from 20 to 100 nm can be measured by DC within 20% experimental error.
(4) DC and SMPS measurements of monodisperse particle surface areas are comparable to a geometric surface area below 100 nm, but they underestimate the geometric surface area in the size range above 100–200 nm. This finding is consistent with the fact that in the transition or continuum regime, these instrument responses depend on active surface area (Fuchs surface area).
(5) For monodisperse aerosol particles smaller than 100 nm, SMPS, TEM, and DC-based measurements of surface area agree.
(6) The results in this study suggest that the DC is a promising instrument for estimating monodisperse ultrafine aerosol surface area, although application to polydisperse aerosol still needs comprehensive experimental validation.

Disclaimer

Mention of any company or product does not constitute endorsement by NIOSH.

Acknowledgements

We would like to thank Amy Feng for providing the statistical test for our data and Anne Votaw for editorial assistance. This research was performed while the author Bon Ki Ku held a National Research Council Research Associateship Award at National Institute for Occupational Safety and Health.

References

Baron, P. A., & Willeke, K. (2001). *Aerosol measurement*: *principles, techniques, and applications* (2nd ed.) (pp. 404–418). New York: Wiley.

Brown, D. M., Wilson, M. R., MacNee, W., Stone, V., & Donaldson, K. (2001). Size dependent proinflammatory effects of ultrafine polystyrene particles: a role for surface area and oxidative stress in the enhanced activity of ultrafines. *Toxicology and Applied Pharmacology*, *175*, 191–199.

Brunauer, S., Emmett, P. H., & Teller, E. (1938). Adsorption of gases in multimolecular layers. *Journal of the American Chemical Society*, *60*, 309–319.

Bukowiecki, N., Kittelson, D. B., Watts, W. F., Burtscher, H., Weingartner, E., & Baltensperger, U. (2002). Real-time characterization of ultrafine and accumulation mode particles in ambient combustion aerosols. *Journal of Aerosol Science*, *33*, 1139–1154.

Friedlander, S. K. (1977). *Smoke, dust, and haze*. New York: Wiley.

Fuchs, N. A. (1963). On the stationary charge distribution on aerosol particles in a bipolar ionic atmosphere. *Geofisica Pura E Applicata*, *56*, 185–193.

Hogg, R. V., & Tanis, E. A. (1993). *Probability and statistical inference* (4th ed.) (p. 456). New York: Prentice-Hall.

Jung, H., & Kittelson, D. B. (2004). Characterization of aerosol surface instruments in transition regime. Personal Communication.

Keller, A., Fierz, M., Siegmann, K., Siegmann, H. C., & Filippov, A. (2001). Surface science with nanosized particles in a carrier gas. *Journal of Vacuum Science and Technology A, Vacuum, Surfaces, and Films*, *19*, 1–8.

Ku, B. K., & Maynard, A. D. (2004). Generation and investigation of airborne silver nanoparticles with specific size and morphology by homogeneous nucleation, coagulation and sintering. *Journal of Aerosol Science*, submitted.

Maynard, A. D. (1995). The development of a new thermophoretic precipitator for scanning transmission electron microscope analysis of ultrafine aerosol particles. *Aerosol Science and Technology*, *23*, 521–533.

Maynard, A. D. (2003). Estimating aerosol surface area from number and mass concentration measurements. *Annals of Occupational Hygiene*, *47*, 123–144.

Oberdörster, G. (2000). Toxicology of ultrafine particles: in vivo studies. *Philosophical Transactions of the Royal Society London Series A*, *358*, 2719–2740.

Oberdörster, G., Gelein, R. M., Ferin, J., & Weiss, B. (1995). Association of particulate air pollution and acute mortality: involvement of ultrafine particles? *Inhalation Toxicology*, *7*, 111–124.

Pui, D. Y. H., Fruin, S., & McMurry, P. H. (1988). Unipolar diffusion charging of ultrafine aerosols. *Aerosol Science and Technology*, *8*, 173–187.

Rogak, S. N., Baltensperger, U., & Flagan, R. C. (1991). Measurement of mass transfer to agglomerate aerosols. *Aerosol Science and Technology*, *14*, 447–458.

Rogak, S. N., & Flagan, R. C. (1992). Bipolar diffusion charging of spheres and agglomerate aerosol particles. *Journal of Aerosol Science*, *23*, 693–710.

Rogak, S. N., Flagan, R. C., & Nguyen, H. V. (1993). The mobility and structure of aerosol agglomerates. *Aerosol Science and Technology*, *18*, 25–47.

Searle, S. R. (1971). *Linear models*. New York: Wiley.

Shi, J. P., Harrison, R. M., & Evans, D. (2001). Comparison of ambient particle surface area measurement by epiphaniometer and SMPS/APS. *Atmospheric Environment*, *35*, 6193–6200.

Siegmann, K., & Siegmann, H. C. (2000). Fast and reliable in-situ evaluation of particles and their surface with special reference to diesel exhaust. *SAE Technical Paper Series* No. 2000-01-1995.

Weber, A. P., Baltensperger, U., Gäggeler, H. W., & Schmidt-Ott, A. (1996). In situ characterization and structure modification of agglomerated aerosol particles. *Journal of Aerosol Science*, *27*, 915–929.

Wilson, W. E., Han, H. S., Stanek, J., Turner, J., & Pui, D. H. Y. (2003). The Fuchs surface area, as measured by charge acceptance of atmospheric particles, may be a useful indicator of the surface area of particles deposited in the lung. *Abstracts of the European Aerosol Conference 2003* (pp. S421–S422). Madrid, Spain.

Woo, K.-S., Chen, D.-R., Pui, D. Y. H., & Wilson, W. E. (2001). Use of continuous measurements of integral aerosol parameters to estimate particle surface area. *Aerosol Science and Technology*, *34*, 57–65.